DOI: 10.1002/ejic.200800047

Template-Free Synthesis, Controlled Conversion, and CO Oxidation Properties of CeO_2 Nanorods, Nanotubes, Nanowires, and Nanocubes

Chengsi Pan,[a] Dengsong Zhang,*[a] Liyi Shi,*[a] and Jianhui Fang[a]

Keywords: Cerium oxide / Ceria / CO oxidation / Nanorods / Nanostuctures / Nanotubes

A general large-scale synthesis of single-crystalline and uniform CeO_2 nanorods was first realized without templates by a precipitation method at room temperature and pressure. Such nanorods have an aspect ratio of ca. 3 nm with a diameter of ca. 8 nm and a large BET specific area of 128.2 m^2/g. On the basis of this, the controlled conversion of the as-prepared nanorods into nanotubes, nanowires, and nanocubes through hydrothermal reactions has been realized. Further experimental results show that the growth of nanorods is a function of the base concentration, temperature, and time. In addition, particle size measurements demonstrate that the primary nanorods grow by Ostwald ripening. It is found that CeO_2 growth is faster at higher base concentration and temperature due to the accelerated ripening. During the synthesis, the formation of $Ce(OH)_3$ intermediate species and their transformation into CeO_2 have been dynamically demonstrated and are regarded as the key factors responsible for the evolution of shape. The CO oxidation properties of CeO_2 nanorods, nanowires, nanotubes, and nanocubes were investigated, and CeO_2 nanotubes have the best performance due to the large BET surface area and the novel inner surface. In addition, CeO_2 nanorods aged for 9 d also have an excellent catalytic performance for CO oxidation due to the exposed crystal surface (110) of CeO_2.

Introduction

Ceria (CeO_2) has been extensively applied in heterogeneous catalysis,[1] solid oxide fuel cells (SOFCs),[2] optics,[3] polishing materials,[4] gas sensors,[5] UV light blockers,[6] and especially in three-way catalysts (TWCs).[7–9] In recent years, one-dimensional CeO_2 nanostructured materials have received a tremendous amount of attention because of their unique properties derived from low dimensionality and a high surface area. Over the past few years, the syntheses of 1-D CeO_2 nanostructured materials with various morphologies, such as nanorods,[10] nanowires,[11] and nanotubes,[12,13] have been carried out by us and other research groups. Recently, remarkable progress has been made in the investigation of their controlled conversion and morphology-dependent properties. For example, Jimmy et al.[14] synthesized CeO_2 spindle-like structures and microspheres by a controllable flux reaction, and found that the former exhibited the higher catalytic activity on CO conversion. Zhang et al.[15] synthesized ceria with various shapes using a controlled hydrothermal method, and experimentally observed that ceria nanorods showed the highest oxygen-storage capacity. Zhou et al.[16] converted CeO_2 nanorods into nanotubes in a H_2O_2 solution assisted by an ultrasonic wave, and the CeO_2 nanotubes showed highly reducible properties. However, exactly controlled synthesis of CeO_2 nanostructures is difficult.

Various routes have been employed to synthesize 1-D CeO_2 nanostructured materials, such as hydrothermal reactions,[17] chemical vapor deposition,[18] and the use of various removable or sacrificial templates.[13,19] However, most of these approaches are energy-consuming or complex. Moreover, it is obvious that complexity and cost will increase greatly when large-scale synthesis of uniform 1D nanostructures is required. Recently, the use of surfactants has proved to be a relatively effective approach. For example, Vantomme et al.[20] obtained CeO_2 nanorods using hexadecyltrimethylammonium bromide (CTAB) as a surfactant at 80 °C under hydrothermal conditions. Gerdanken et al.[21] synthesized α-Fe_2O_3, CuO, and ZnO nanorods by using octylamine at 80 °C with agitation. Tang et al.[22] obtained α-FeOOH nanorods simply by a liquid-phase deposition method, which were then converted into α-Fe_2O_3 under hydrothermal conditions. Recently, we also synthesized CeO_2 nanorods and nanotubes using CTAB as a surfactant under hydrothermal conditions.[23] Nevertheless, the removal of the surfactant is still a problem because of the strong force between the reagent and favorable crystal surfaces. Thus, the development of a facile and template-free method to create CeO_2 one-dimensional nanostructures is of great significance. Moreover, the template-free synthesis of 1-D CeO_2 nanostructured materials under an ambient condition is still a challenge.

[a] Research Center of Nano Science and Technology and Department of Chemistry, Shanghai University,
Shanghai, 200444, China
Fax: +86-21-66134852
E-mail: dszhang@shu.edu.cn
Supporting information for this article is available on the WWW under http://www.eurjic.org or from the author.

Recently, we synthesized CeO_2 nanorods assisted by PEG600 as a capping reagent with an ultrasonic wave method[10] and CeO_2 nanotubes assisted by carbon nanotubes with a liquid-phase deposition method.[13] Herein, we first report on a liquid precipitation method to synthesize single-crystal CeO_2 nanorods at room temperature and pressure, without stirring or titrating. On the basis of this, the controlled conversion of nanorods into nanotubes, nanowires, and nanocubes under hydrothermal conditions is also discussed. Enhanced catalytic activity was seen for CO oxidation when using CeO_2 nanorods and nanotubes as compared to CeO_2 nanoparticles.

Results and Discussion

Characteristics of CeO_2 Nanorods

Figure 1 shows the XRD pattern of CeO_2 nanorods. The sample exhibits peaks that correspond to the (111), (200), (220), (311), (400), (331), and (420) planes of a cubic fluorite structure (space group: *Fm*3*m*) of CeO_2 as identified using the standard data JCPDS 78–0694. The value of the lattice parameter calculated from the XRD spectra is 0.53439 nm, which is lower than that reported for the bulk CeO_2 (0.54113 nm) in the standard data JCPDS 78–0694. The hydroxy groups may stabilize the small nanoparticles resulting in the smaller value of the lattice parameter in our sample, which is similar to the result reported by Maensiri et al.[24] The ideal intensity ratio of a CeO_2 crystal between the (200) and (220) reflection approaches 0.6, while the measured ratio in this experiment is smaller than 0.4. This phenomenon suggests that the present CeO_2 crystals may grow along the [220] axis, which has also been observed for some other 1D materials.[25]

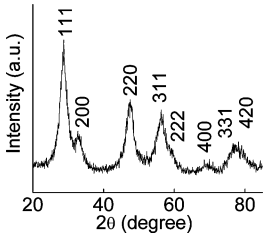

Figure 1. XRD pattern of CeO_2 nanorods synthesized at 20 °C for 24 h.

Figure 2 shows the TEM and HRTEM images of CeO_2 nanorods at different scales, which show that the as-prepared sample is 30 ± 10 nm in length and 7.5 ± 2.5 nm in width. All the images show that CeO_2 nanorods have a uniform structure. Parts a and b in Figure 2 show that most of the CeO_2 nanorods are easily aggregated. The HRTEM (Figure 2, c) image shows that most of the CeO_2 nanorods (>98%) are not rectangular in structure but polyhedral on their tips. Figure 2 (d) displays a cross-lattice pattern with a lattice spacing of 0.19 nm, corresponding to the interplanar separation between the {220} or {022} lattice planes of cubic ceria, which implies ceria nanorods grow along the [110] direction, and this result is in agreement with the XRD analysis presented in this work.

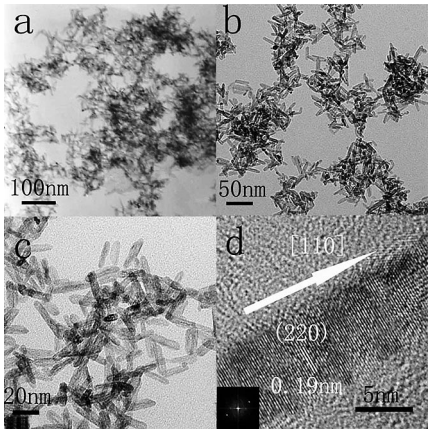

Figure 2. Typical TEM (a and b) and HRTEM (c and d) images of CeO_2 nanorods synthesized at 20 °C for 24 h. Inset is the FFT pattern of d.

Pure CeO_2 is a white powder, but our product is yellow, which indicates that the composition may be CeO_{2-x}, where $0 < x < 0.5$. Replacement of the smaller Ce^{4+} ions by the larger Ce^{3+} ions may result in the color change.[26] To further confirm this result, an XPS spectrum (Figure 3) was recorded. The wide spectrum (Figure 3, a) of nanorods reveals the predominant presence of cerium, oxygen, and carbon. No other heteroelements, including sodium and nitrogen, are observed, which suggests that there are no unreacted precursors in the composites. The 3d signal of the Ce sample corresponds to that of both Ce^{IV} and Ce^{III} in CeO_2. According to the assignment proposed by Burroughs et al.,[27] the 3d3/2 multiplet signals of Ce^{IV} are labeled u, u′′, and u′′′, while those of 3d5/2 are labeled v, v′′, and v′′′. The Ce^{III} signal always exhibits four peaks (U_0, U′, V_0, and V′),[28] and two features are obviously located at around 906 and 886 eV as shown in part b of Figure 3.

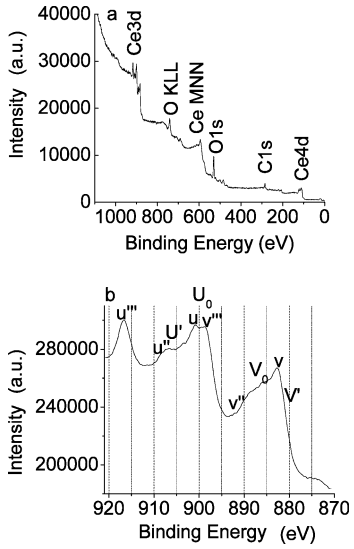

Figure 3. XPS wide spectrum (a) and Ce3d spectrum (b) of CeO_2 nanorods synthesized at 20 °C for 24 h.

Conversion of CeO_2 Nanorods Into Nanotubes, Nanowires, and Nanocubes

The CeO_2 nanorods obtained at room temperature and pressure are a good precursor and can be easily converted into other nanostructures. Further experiments show the controlled conversion of nanorods into nanotubes, nanowires, and nanocubes can be realized by changing the reaction time and temperature under hydrothermal conditions.

Figure 4 shows the evolution of CeO_2 nanorods under various hydrothermal conditions. CeO_2 nanorods are converted into nanotubes with a size of 50×200 nm, at 100 °C for 72 h (Figure 4, a). The length of the nanotubes is the same as that of the nanorods synthesized at 100 °C for 24 h, while the diameter is nearly twice that of the rods, which indicates that recrystallization on the surface may also accompany a "dissolution" process. The conversion process may initiate etching from the center of the nanorods to form nanotubes, which is similar to that which occurs in Fe_2O_3.[29]

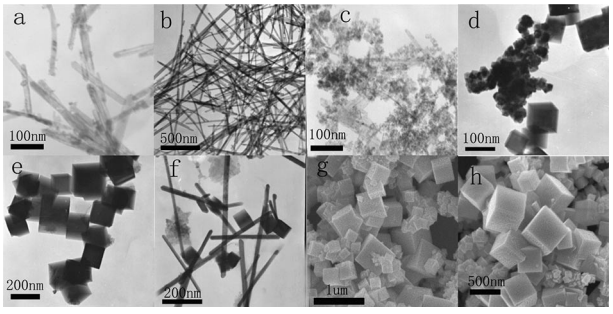

Figure 4. TEM images of the conversion of CeO_2 nanorods under various hydrothermal conditions: (a) nanotubes (100 °C, 72 h), (b) nanowires (110 °C, 24 h), (c) nanoparticles (120 °C, 24 h), (d) nanoparticles and nanocubes (140 °C, 24 h), (e) nanocubes (160 °C, 24 h), (f) nanocubes, nanoparticles, and nanorods (180 °C, 2 h), and (g, h) nanocubes (180 °C, 24 h).

CeO_2 nanorods are converted into nanowires (Figure 4, b) with an aspect ratio of ca. 40 at 110 °C for 24 h. The diameter of the CeO_2 nanowires is ca. 25 nm, equal to that of nanorods synthesized at 100 °C for 24 h, which implies the growth from nanorods into nanowires along the axis.

At 120 °C for 24 h, CeO_2 nanowires are converted into nanoparticles with a size of ca. 15 nm (Figure 4, c), which also can be obtained at 110 °C for 72 h, indicating that CeO_2 nanowires have a limit on growth. The growth process is limited by some conditions such as the oxidation of $Ce(OH)_3$ to CeO_2.

At 140 °C, 160 °C, and 180 °C for 24 h, CeO_2 nanorods are converted into nanocubes (Figure 4, d, e, g, h), the sizes of which are 100 nm, 200 nm, and 500 nm, respectively. At 180 °C for 2 h, CeO_2 nanorods, nanocubes, and nanoparticles are obtained at the same time (Figure 4, f), which implies the nanorod–nanoparticle–nanocube conversion mechanism.

The phase purity of CeO_2 nanotubes, nanowires, and nanocubes obtained was also examined by XRD (Figure 5). All the samples can be indexed as a face-centered cubic phase (space group: *Fm*3*m*) of ceria (JCPDS no. 78–0394). Of all the samples, the CeO_2 nanocubes exhibit the highest intensity indicating the best crystalline form.

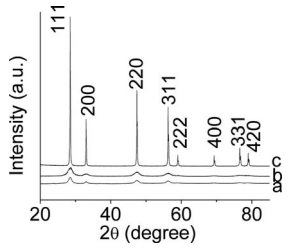

Figure 5. XRD patterns of the as-prepared CeO_2 nanostructures: (a) nanotubes, (b) nanowires, and (c) nanocubes synthesized at 180 °C for 24 h.

The pore size distribution of CeO_2 nanostructures is shown in Figure 6. It is obvious that the distribution curve of the nanotubes has two peaks: one is at 4.2 nm, and the other is at 20.4 nm. The former is caused by the open ends of the nanotubes, while the latter is attributed to stacking of the nanotubes. The average pore volume of the nanowires is somewhat larger than that of the nanorods synthesized at 100 °C for 24 h, because of the length difference. It is noted that CeO_2 nanocubes have the smallest pore volume due to a compact structure.

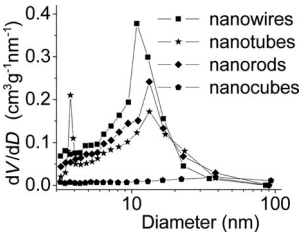

Figure 6. The pore-size distribution plots for various CeO_2 nanostructures (nanorods synthesized at 100 °C for 24 h, and nanocubes synthesized at 180 °C for 24 h). The average relative standard deviation of rod diameter was 2%.

Synthesis Factors and Formation Mechanism of CeO_2 Nanostructures

The experimental results show that the formation of CeO_2 nanostructures can be divided into two steps: growth and evolution of nanorods. The latter is strongly influenced by the former. We changed the synthesis conditions for nanorods to investigate the formation mechanism of CeO_2 nanorods and other nanostructures.

Figure 7 shows the impact of NaOH concentration on the growth of nanorods. When the NaOH concentration decreases from 14 to 7 M (Figure 7, a), nanorods with a poor crystalline form are obtained. When a concentration of 1 M is reached (Figure 7, b), nanorod structures with a poorer crystalline form accompanied by a few nanoparticles (<20%) are obtained. At pH = 10 and pH = 7 (Figure 7, c, d), nanorods are not obtained but irregular particles with

a size of 10–20 nm. It is interesting that the rates at which nanorods grow by consuming nanoparticles significantly accelerates with increasing NaOH concentration (Figure 7).

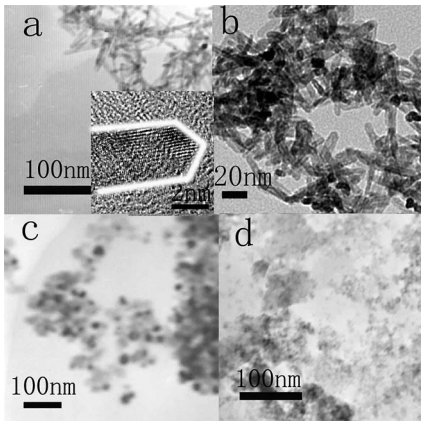

Figure 7. TEM images of CeO_2 nanorods prepared at 20 °C for 24 h under various NaOH concentrations: (a) 6 M, (b) 1 M, (c) pH = 10, and (d) pH = 7. Inset is an HRTEM image for nanorods (white line) prepared under 6 M NaOH at 20 °C for 24 h.

Figure 8 shows the evolution of particle width, length, and aspect ratio as a function of time. At the beginning (Figure 8, a), the fast conversion of nanoparticles into nanorods at room temperature is observed, this being even faster at higher temperature (Figure S1). After 6 h, the sample consists mostly of randomly oriented ceria nanorods (Figure 8, b). As the reaction advances, the nanorod length and width remain constant (5–10 nm in diameter and 25–35 nm in length) (Figure 8, c, d), suggesting that once the nanorods reach a certain average size, the existing nanorods almost cease growing. HRTEM images (Figure 8, d, f) show

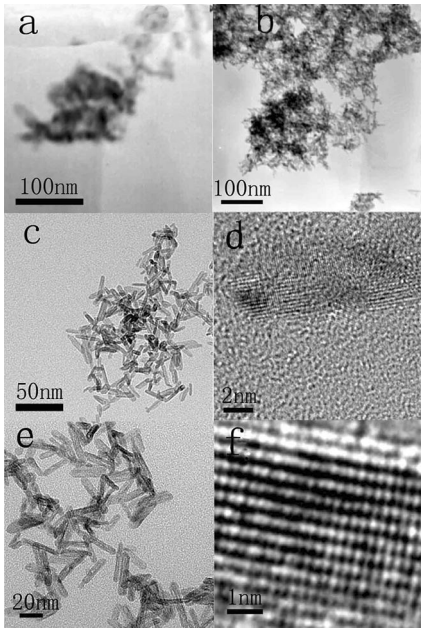

Figure 8. TEM and HRTEM images of CeO_2 nanorods prepared at 20 °C for various aging times: (a) 0 h, (b) 6 h, (c, d) 12 h, and (e, f) 9 d.

that the CeO_2 crystalline form reaches perfection after aging for 9 d, though the nanorod length is almost the same (Figure 8, e, f). Particle size analysis shows that the nanorods grow at the expense of the primary particles and demonstrates that coarsening is an important growth mechanism in this system (discussed below).

Figure 9 shows representative TEM images of samples aged at 40, 60, 80, and 100 °C for 24 h. In general, ceria nanorods have an increasing aspect ratio at higher temperature: average sizes are 8.0×50 nm for 40 °C, 10×70 nm for 60 °C, 13×105 nm for 80 °C, and 25×300 nm for 100 °C, respectively. Not surprisingly, the rate of ceria nanorod formation increases with increasing aging temperature (Figure 9). The size and shape data of the nanorods aged at 40 and 80 °C are presented in Figure 10, which details the morphology of ceria nanorods as a function of aging time and temperature. It is found that the width of the nanorods aged at 40 or 80 °C changes little over time despite the obvi-

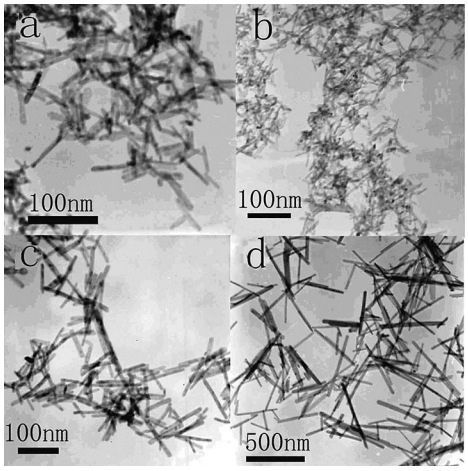

Figure 9. TEM images of CeO_2 nanorods prepared at various temperatures for 24 h: (a) 40 °C, (b) 60 °C, (c) 80 °C, and (d) 100 °C.

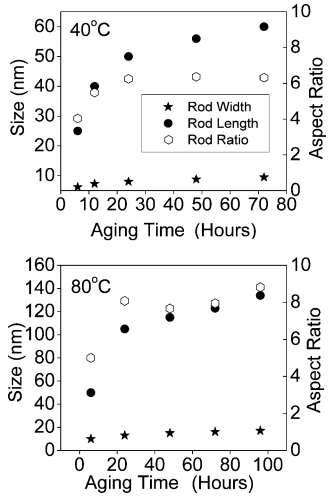

Figure 10. Plots of rod width, length, and aspect ratio against aging time for particles aged at 40 (top), and 80 °C (bottom). The average relative standard deviation of rod width, length, and aspect ratio was 32%.

ous increase in length. However, at an elevated temperature (100 °C), the nanorods increase sharply in width over time. The aspect ratio distribution reveals a single peak at ca. 24 h, which implies the growth limitation for nanorods.

Particle size analysis (Figure 11) suggests that these nanorods grow by coarsening. Coarsening, also known as Ostwald ripening, is a mechanism driven by the high chemical potential of nanoparticles, described by the Gibbs–Thompson equation. A rate law for this process is developed by inserting the linearized Gibbs–Thompson equation into Fick's first law as shown in Equation (1);[30,31] $r_{<Ü–>}$ is the average particle size at time t, $r_{<Ü–>0}$ is the average initial particle size, and k is the rate constant. This rate law is commonly used to describe diffusion-limited particle growth in the solid state and in liquids. Thus, larger particles grow at the expense of smaller particles by diffusion of molecular-scale species through solution.[32,33]

$$\bar{r}^3 - \bar{r}_0^3 = kt \tag{1}$$

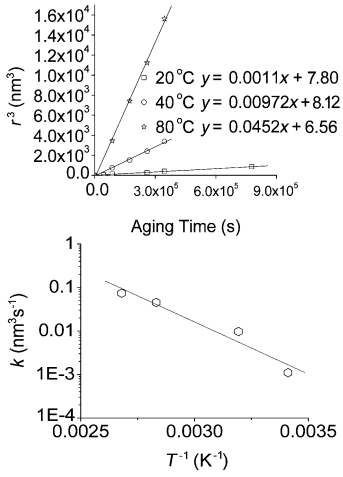

Figure 11. (a) Plot of the average primary nanoparticle radius cubed (r^3) vs. aging time. Particles were synthesized aged at 20, 40, and 80 °C. Solid lines represent linear fits, which were determined by the least-squares method. (b) The rate constant k vs. reciprocal temperature for the coarsening of CeO_2 particles. The average relative standard deviation of rod width, length, and aspect ratio was 32%.

Average r^3 increases with aging time for each of the temperature series, and linear fits are good for all the 20, 40, and 80 °C datasets (Figure 11, a), which suggests that CeO_2 nanorods grow by Ostwald ripening. The rate constant k, obtained from the slopes of the linear regions of the plots of $r_{<Ü–>3}$ vs. time, is in the range of 10^{-3}–10^{-2} $nm^3 s^{-1}$ and increases with the aging temperature. The activation energies obtained from the slope (Figure 11, b) is 1.60 $kJ mol^{-1}$.

The ideal coarsening kinetics (Table S1) for CeO_2 can be determined by Equation (2);[32] η is the viscosity of the solvent, a is the solvated ion radius, Vm is the molar volume, $c_{r=\infty}$ is the equilibrium concentration, NA is Avogadro's number, and γ is the surface energy.

$$k = \frac{8\gamma V_m^2 c_{r=\infty}}{54\pi\eta a N_A} \tag{2}$$

The surface energy for the solid–vapor interface for metal oxides is of the order of 1 $J m^{-2}$.[34–37] However, electrostatic and chemical interactions at the solid–liquid interface are expected to reduce the surface energy to values in the range 0.1–0.5 $J m^{-2}$.[38] Taking r = 0.1 $J m^{-2}$, the ideal rate constant obtained is between 10^{-8} and 10^{-10} $nm^3 s^{-1}$ (Table S1), which is far from the experimental results. However, when $Ce(OH)_3$ replaces CeO_2, the ideal rate constant is between 10^{-2} and 10^{-3} $nm^3 s^{-1}$ (Table S1), which is in the same class as the experimental results (Figure 11, a). The difference between the two results is caused by the difference in solubility, which is 5.23×10^{-12} $mol L^{-1}$ for CeO_2 and 4.85×10^{-6} $mol L^{-1}$ for $Ce(OH)_3$. Though the phase detection for $Ce(OH)_3$ is hard due to the easy conversion between Ce^{3+} and Ce^{4+},[7] this result still gives a dynamic demonstration of the $Ce(OH)_3$ growth mechanism. When $Ce(NO_3)_3$ is replaced by $(NH_4)_2Ce(NO_3)_6$, CeO_2 nanorods are not obtained (Figure S2), which indicates the Ce^{3+} ions also play an important role in nanorod growth. Recently, Tang et al.[25] demonstrated the phase of $Ce(OH)_3$ intermedia species via XRD under the base condition by using N_2 as the protected gas for the whole experimental and detection procedures.

According to the above results, we conclude that the $Ce(OH)_3$ particles form first. The hydroxy groups limit the lateral growth, and then the primary nanorods form. The sides of the nanorods may be oxidized easily by oxygen in solution due to the large interface surface, which also limits lateral growth.

Combining the nanorod growth mechanism with the experimental results, the conversion procedures are suggested in Scheme 1. Two reactions occur during the hydrothermal reaction: one is the oxidation of the dissolved Ce^{3+} to Ce^{4+}; the other is the growth of the nanorods. $k1$ is used as the rate constant of the former, and $k2$ is used for the latter. As discussed, the sides of the nanorods mainly consist of CeO_2, which limits the nanorod growth, while the inner parts of the nanorods mainly consist of $Ce(OH)_3$, which promotes nanorod growth. When $k1 > k2$, the main reaction is that the dissolved Ce^{3+} is oxidized in solution and then preferen-

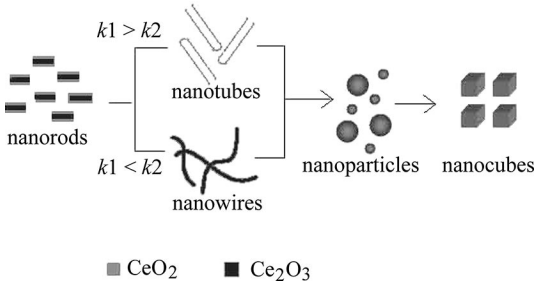

Scheme 1. Possible conversion mechanism for CeO_2 nanorods. $k1$ is represented as the rate constant of the oxidation of the dissolved Ce^{3+} to Ce^{4+} and $k2$ is represented as the rate constant of the growth of CeO_2 nanorods.

tially deposits on the surface of the nanorods. Thus, CeO_2 nanotubes can be obtained at the appropriate time and temperature. When $k1 < k2$, the Ce^{3+} ions prefer to deposit on the tips of the nanorods, which results in the formation of CeO_2 nanowires. At higher temperatures, the oxidation occurs not only at the surface, but also in the bulk, which breaks the nanowires. With rising temperature, CeO_2 nanoparticles grow into nanocubes with characteristics as reported by Yan et al.[15]

CO Catalytic Oxidation of CeO_2 Nanostructures

Herein, the catalytic activities of CeO_2 were compared to the temperature (T_{50}) at which 50% CO was converted to CO_2.

Figure 12 and Figure S3 show that the catalytic activity of CeO_2 nanorods is influenced by the aging time and temperature. It is clear that all the nanorods become more active as the aging time increases. The CO oxidation activity of nanorods synthesized at 20 °C shows the largest change, and with increasing aging time, the T_{50} approaches that of the samples synthesized at 40 °C or 80 °C that have aged for the same time period. It is well known that the large BET specific area benefits the catalytic reaction. It is noted that CeO_2 nanorods synthesized at 20 °C possess not the highest catalytic activity but the largest BET specific area. Previous computer modeling shows that the energy required to form oxygen vacancies on (110) and (100) is less than that on (111).[39] Recently, Zhou et al.[17] reported that the CO oxidation activity of CeO_2 was strongly influenced by the crystal plane due to varying ability for creating oxygen vacancies, which was also the key point for CO oxidation. For shorter aging times (0–24 h), the crystal surface is the key factor due to the obvious difference of crystalline form for nanorods synthesized at 20, 40, and 80 °C. As the aging time increases, the crystalline form does not vary much, and then at a certain point the BET specific area becomes the key factor. Thus, the T_{50} of samples synthesized at the lowest temperature is the lowest because they have the largest BET specific area (ca. 120.3 m^2/g). It is obvious that the nanorods synthesized at low temperature with enough aging time can possess a large BET specific area and a perfect crystalline form and thus have a high performance for CO oxidation.

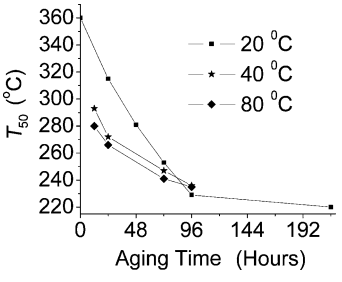

Figure 12. Plot of the T_{50} vs. aging time for CeO_2 nanorods synthesized at 20 °C, 40 °C, and 80 °C. The average relative standard deviation of T_{50} was 2%.

Table 1 and Figure S4 show catalytic activities of CeO_2 nanotubes, nanorods (20 °C for 24 h and 9 d), nanowires, nanoparticles, and nanocubes. The order of T_{50} for CeO_2 for the various nanostructures is as follows: nanotubes < nanorods (20 °C for 9 d) < nanowires < nanorods (20 °C for 24 h) < nanoparticles < nanocubes. This is confirmed by the conversion rate of CeO_2 nanostructures at 300 °C in Table 1. The BET specific area is also listed for contrast. The excellent catalytic properties of CeO_2 nanotubes could be explained by the combination of the large surface-to-volume area with the inner parts of the nanotubes providing more active sites for CO oxidation. CeO_2 nanocubes have the lowest activity because they have the largest particle size (ca. 100 nm) and the smallest BET specific area. The CO oxidation activity of the nanowires is higher than that of nanorods synthesized at 20 °C for 24 h because of the superior crystalline form, while at the same time less than that of nanorods synthesized at 20 °C for 9 d because of the smaller BET specific area. The catalytic activity of nanoparticles is lower than that of 1D nanostructures due to the main plane (111) which is regarded as the least reactive crystal surface.[40,41] Therefore to summarize, the large BET specific area and the favorable crystal surface of CeO_2 are good for the catalytic reaction of CO oxidation.

Table 1. BET specific area and catalytic activity of CeO_2 nanostructures.

Sample	T_{50} [°C]	Conversion rate at 300 °C [μmol/(g s)]	S_{BET} [m^2/g][d]
Nanorods[a]	290	1.13	128.2
Nanorods[b]	224	1.79	115.9
Nanoparticles	305	0.933	105.1
Nanowires	245	1.63	79.8
Nanotubes	223	1.81	98.2
Nanocubes[c]	315	0.655	3.5

[a] CeO_2 nanorods synthesized at 20 °C for 24 h. [b] CeO_2 nanorods synthesized at 20 °C for 9 d. [c] CeO_2 nanocubes synthesized at 180 °C for 24 h. [d] The average relative standard deviation of S_{BET} was <5%.

Conclusions

In summary, a large-scale synthesis of single-crystalline and uniform CeO_2 nanorods has been realized by a liquid deposition method at room temperature and pressure using some cheap and simple sources, such as NaOH and $Ce(NO_3)_3 \cdot 6H_2O$. Experimental results show that the growth of nanorods is a function of the base concentration, temperature, and time. On the basis of this, the conversion of the as-prepared nanorods into nanotubes, nanowires, and nanocubes through hydrothermal reactions has been realized. The transformation of $Ce(OH)_3$ into CeO_2 has been dynamically demonstrated and is regarded as the key factor responsible for the evolution of shape. The CO oxidation properties of CeO_2 nanorods, nanowires, nanotubes, and nanocubes have been investigated. CeO_2 nanorods synthesized at low temperature with enough aging time can possess a large BET specific area and a perfect crystalline form

and thus have a high performance for CO oxidation. We believe that these structural characteristics of CeO_2 are likely to affect their performance in catalysis and can be extended to other technological applications.

Experimental Section

Synthesis of CeO_2 Nanorods: Analytical grade $Ce(NO_3)_3·6H_2O$ and NaOH were purchased from Shanghai National Chemical Company and were used without further purification. The reaction was carried out in a 50-ml capacity Teflon-lined stainless steel autoclave, and in a digital temperature-controlled oven.

In a typical procedure, $Ce(NO_3)_3·6H_2O$ solution (16 mmol, 5 mL) and NaOH solution (14 M, 35 mL) were mixed in a beaker, without stirring or titrating. The suspension was then left at room temperature (20 °C) and pressure for 24 h. The product was washed three times with distilled water and dried at 80 °C for 24 h.

To follow growth as a function of base concentration, at 20 °C for 24 h, the base concentration was adjusted to 7 M, 1 M, pH = 10, pH = 7. To determine the effect of the aging temperature and time, a series of experiments was carried out: at 20 °C, the aging time was adjusted to 0, 12, 48, 72, 96, and 216 h; at 40 °C, the aging time was adjusted to 2, 6, 12, 24, 48, 72, and 96 h; and at 80 °C, the aging time was adjusted to 6, 24, 48, 72, and 96 h. At 100 °C, the suspension was transferred into a 50-mL capacity Teflon-lined stainless steel autoclave, and then left for 6, 12, and 24 h.

Conversion of CeO_2 Nanorods into Other Nanostructures: In a typical procedure, $Ce(NO_3)_3·6H_2O$ solution (16 mmol, 5 mL) and NaOH solution (14 M, 35 mL) were mixed in a beaker at room temperature and pressure, without stirring or titrating. The suspension was then transferred into a 50-mL capacity Teflon-lined stainless steel autoclave. The autoclave was set at 100 °C for 72 h, 110 °C for 24 h, 120 °C for 24 h, 120 °C for 72 h, 140 °C for 24 h, 160 °C for 24 h, 180 °C for 2 h, and 180 °C for 24 h, and various CeO_2 nanostructures were obtained.

Evaluation of Catalytic Activity: The catalytic activities for CO oxidation were evaluated in a U-shaped quartz reactor. The catalyst particles (0.15 g) were placed in the reactor. The reactant gases (1.0% CO, 28% O_2, balanced with nitrogen) passed through the reactor at a rate of 40 mL/min. The composition of the gas exiting the reactor was monitored by gas chromatography, to determine both the removal of CO and the formation of CO_2; the conversions were determined on the basis of CO consumption and CO_2 formation with a detection limit for CO evaluation of 0.5‰. All the catalytic results were repeated three times at a given temperature. An on-line gas chromatograph (GC508A) equipped for column switching (activated carbon and molecular sieves) in combination with a thermal conductivity detector was used to analyze the gas stream.

Material Characterization: The as-prepared CeO_2 nanotubes were characterized by XRD (Rigaku D/max2500PC) with Cu-K_a radiation, SEM (JEOL, JSM-6700F), TEM (JEOL, JEM-2010), HRTEM (Hitachi-9000 NAR, accelerating voltage of 300 kV), and Brunauer–Emmett–Teller nitrogen adsorption–desorption (Micromeritics ASAP 2020) measurements. For TEM and HRTEM measurements, powdered samples were dispersed in absolute ethanol by ultrasonication for 10 min in a KQ-250B ultrasonic bath, after which a single drop of the resulting suspension was placed onto a 200 mesh holey carbon-coated copper grid (SPI), which was then allowed to dry in air. The probe size for TEM was 2–5 nm in diameter, and that for HRTEM was 0.13 nm in diameter. XPS was performed with an ESCALab 220i-XL spectrometer at a pressure of about 3×10^{-9} mbar (1 mbar = 100 Pa) using Al-K_α as the excitation source (hm = 1486.6 eV) and operating at 15 kV and 20 mA.

Supporting Information (see also the footnote on the first page of this article): TEM images of CeO_2 nanorods aging at various times and temperatures, TEM image of CeO_2 synthesized by replacing $Ce(NO_3)_3$ with $(NH_4)_2Ce(NO_3)_6$, plots of CO conversion rate vs. temperature for various CeO_2 nanostructures, and the ideal rate constants for $Ce(OH)_3$ and CeO_2.

Acknowledgments

The authors acknowledge the support of the Innovative Team Project of the Science and Technology Commission of Shanghai, China (06DZ05902) and Shanghai Special Foundation for Selected Cultivation of Excellent Young University Teachers (shu-07048). The authors would like to thank Dr Q. Li and Y. L. Chu for help with the TEM and SEM measurements.

[1] B. Murugan, A. V. Ramaswamy, *J. Am. Chem. Soc.* **2007**, *129*, 3062–3063.
[2] H. Y. Yahiro, K. Baba, H. Eguchi, J. Arai, *Electrochem. Soc.* **1988**, *135*, 2077–2080.
[3] H. Gu, M. D. Soucek, *Chem. Mater.* **2007**, *19*, 1103–1108.
[4] X. D. Feng, D. C. Sayle, Z. L. Wang, M. S. Paras, B. Santora, A. C. Sutorik, T. X. T. Sayle, Y. Yang, Y. Ding, X. D. Wang, Y. S. Her, *Science* **2006**, *312*, 1504–1508.
[5] N. Izu, W. Shin, N. Murayama, S. Kanzaki, *Sens. Actuator, B* **2002**, *87*, 95–98.
[6] S. Tsunekawa, T. Fukuda, A. Kasuya, *J. Appl. Phys.* **2000**, *87*, 1318–1321.
[7] A. Trovarelli, *Catal. Rev. Sci. Eng.* **1996**, *38*, 439–520.
[8] J. Kašpar, P. Fornasiero, M. Graziani, *Catal. Today* **1999**, *50*, 285–298.
[9] M. L. Granados, F. C. Galisteo, P. S. Lambrou, R. Mariscal, J. Sanzc, I. Sobrados, J. L. G. Fierro, A. M. Efstathiou, *J. Catal.* **2006**, *239*, 410–421.
[10] D. S. Zhang, H. X. Fu, L. Y. Shi, C. S. Pan, Q. Li, Y. L. Chu, W. J. Yu, *Inorg. Chem.* **2007**, *46*, 2446–2451.
[11] B. Tang, L. Zhuo, J. Ge, G. Wang, Z. Shi, J. Niu, *Chem. Commun.* **2005**, 3565–3567.
[12] W. Q. Han, L. Wu, Y. Zhu, *J. Am. Chem. Soc.* **2005**, *127*, 12814–12815.
[13] D. S. Zhang, H. X. Fu, L. Y. Shi, J. H. Fang, Q. Li, *J. Solid State Chem.* **2007**, *180*, 654–660.
[14] C. Ho, J. C. Yu, T. Kwong, A. C. Mak, S. Lai, *Chem. Mater.* **2005**, *17*, 4514–4522.
[15] H. X. Mai, L. D. Sun, Y. W. Zhang, R. Si, W. Feng, H. P. Zhang, H. C. Liu, C. H. Yan, *J. Phys. Chem. B* **2005**, *109*, 24380–24385.
[16] K. Zhou, Z. Yang, S. Yang, *Chem. Mater.* **2007**, *19*, 1215–1218.
[17] K. Zhou, X. Wang, X. Sun, Q. Peng, Y. Li, *J. Catal.* **2005**, *229*, 206–212.
[18] D. Barreca, A. Gasparotto, C. Maccato, C. Maragno, E. Tondello, *Langmuir* **2006**, *22*, 8639–8641.
[19] H. P. Yang, D. S. Zhang, L. Y. Shi, J. H. Fang, *Acta Mater.* **2008**, *56*, 955–967.
[20] A. Vantomme, Z. Y. Yuan, G. Du, B. L. Su, *Langmuir* **2005**, *21*, 1132–1135.
[21] Z. Zhong, M. Lin, N. Vivien, N. G. X. Boon, Y. Foo, A. Gedanken, *Chem. Mater.* **2006**, *18*, 6031–6036.
[22] B. Tang, G. Wang, L. Zhuo, J. Ge, L. Cui, *Inorg. Chem.* **2006**, *45*, 5196–5201.
[23] C. S. Pan, D. S. Zhang, L. Y. Shi. *J. Solid State Chem.* **2008**, DOI: 10.1016/j.jssc.2008.02.011, in press.

[24] S. Maensiri, C. Masingboon, P. Laokul, W. Jareonboon, V. Promarak, P. L. Anderson, S. Seraphin, *Cryst. Growth Des.* **2007**, *7*, 950–955.
[25] C. Tang, Y. Bando, B. Liu, D. Golberg, *Adv. Mater.* **2005**, *17*, 3005–3009.
[26] F. Zhang, S. Chan, J. E. Spanier, E. Apak, Q. Jin, R. D. Robinson, I. P. Herman, *Appl. Phys. Lett.* **2002**, *80*, 127–129.
[27] P. Burroughs, A. Hamnett, A. F. Orchard, G. Thornton, *J. Chem. Soc., Dalton Trans.* **1976**, *17*, 1686–1691.
[28] R. D. Mullins, *Surf. Sci.* **1998**, *409*, 307–309.
[29] C. J. Jia, L. D. Sun, Z. G. Yan, L. P. You, F. Luo, X. D. Han, Y. C. Pang, Z. Zhang, C. H. Yan, *Angew. Chem. Int. Ed.* **2005**, *44*, 4328–4333.
[30] I. M. Lifshitz, V. V. Slyozov, *J. Phys. Chem. Solids* **1961**, *19*, 35–49.
[31] C. Wagner, *Elektrochem.* **1961**, *65*, 581–591.
[32] G. Oskam, Z. Hu, R. L. Penn, N. Pesika, P. C. Searson, *Phys. ReV. E* **2002**, *66*, 011403–1-011403–8.
[33] D. J. Burleson, R. L. Penn, *Langmuir* **2006**, *22*, 402–409.
[34] A. A. Gribb, J. F. Banfield, *Am. Mineral.* **1997**, *82*, 717–728.
[35] X. G. Wang, W. Weiss, S. K. Shaikhutdinov, M. Riter, M. Petersen, F. Wagner, R. Schlögl, M. Scheffler, *Phys. Rev. Lett.* **1998**, *81*, 1038–1041.
[36] I. Manassidis, A. D. Vita, M. J. Gillan, *Surf. Sci. Lett.* **1993**, *285*, 517–523.
[37] D. A. Weirauch, P. D. J. Ownby, *J. Adhes. Sci. Technol.* **1999**, *13*, 1321–1325.
[38] A. Zangwill, *Physics at Surfaces*, Cambridge University Press, Cambridge, **1988**, p. 223.
[39] J. C. Conesa, *Surf. Sci.* **1995**, *339*, 337–352.
[40] T. X. T. Sayle, S. C. Parker, C. R. A. Catlow, *Surf. Sci.* **1994**, *316*, 329–336.
[41] D. C. Sayle, S. A. Maicaneanu, G. W. Watson, *J. Am. Chem. Soc.* **2002**, *124*, 11429–11439.

Received: January 15, 2008
Published Online: April 17, 2008

